Progress In Electromagnetics Research, PIER 45, 313–333, 2004

NEAR FIELD AND SURFACE FIELD ANALYSIS OF THIN WIRE ANTENNA IN THE PRESENCE OF CONDUCTING CUBE

X. J. Zhang, A. Q. Liu, Y. H. Lee, and A. Alphones

School of Electrical & Electronic Engineering
Nanyang Technological University
Nanyang Avenue, Singapore 639798

C. H. Liang

Department of Electrical Engineering
Xidian University
Xi'an 710071, P. R. China

Abstract—The electric field integral equation (EFIE) with the method of moments (MoM) is used for treating problems of a thin wire antenna in the presence of a conducting cube. Pulse-expansion and point-matching technique in MoM are applied to both thin wire and closed object. For simplicity and efficiency, hybrid method for calculating near field and more importantly the surface field of objects is presented. Several examples in this paper show the validity of the proposed pulse-expansion and point-matching technique and the simplified hybrid calculation method.

1. INTRODUCTION

In a complex electromagnetic environment, such as ships, aircraft and other vehicles, surface and near field analysis is of practical and theoretical interest. There are various numerical methods available to calculate these fields. It is a common principle that the surface tangential electric fields are zero on perfect conductors when excited by electromagnetic fields. Due to the inherent numerical errors of computational methods, the surface tangential electric fields may not be exactly zero on perfect conductors. One can easily find out which numerical method is more accurate by comparing the resulting surface tangential electric fields distribution on the surfaces of perfect conductors. The method whose surface tangential electric field distribution is more close to zero gives a more accurate estimation to the solution of the problem.

The moment method (MoM) is a proven technique to solve far field problems such as radiation pattern and Radar Cross Section (RCS). Glisson [1] modeled the surface of open objects by using rectangular patch model, and reported only the current distribution on several open objects such as conducting strips, and rectangular conducting bend structures etc. Rao [2] presented the current distribution with the planar triangular patch model that was later extended by Wilkes and Cha [3] to the curved triangular patch.

When wire and surface currents are obtained using the MoM, it becomes more difficult to solve near field problems since the size of wire current units or surface current patches is comparable to the distance between source and observation point. There is a need to develop a novel technique for the calculation of the near field numerically rather than integrally. Furthermore, when the observation point is located on the conducting object, the surface fields cannot be obtained due to the integral's singularity. Fortunately, Erich Kemptner [4] presented an analytical method to treat the singular terms of the integrals when calculating the surface fields of conducting bodies. However, the low computational efficiency is not acceptable when calculating an entire region by numerical integration.

In this paper, the Glisson patch model is extended to the application of closed objects such as conducting cubes by using the pulse expansion and point matching procedure in the MoM. By the appropriate treatment of singular properties, the surface current density is obtained. The Series Electric Dipole Method (SEDM) [5] is then used to model the wire current units and surface current patches. A hybrid method that combines the SEDM and the Eric Kemptner Method to improve the computational efficiency is presented.

2. FORMULATION USING EFIE AND MOM

2.1. Segmentation of the Objects

A thin wire antenna in the presence of a conducting cube is shown in Fig. 1. The cube is divided into m_x, m_y, m_z segments in the x, y, z direction respectively. There are three directions for the current flowing on the surface as shown in Fig. 2, which are called s_x, s_y, s_z respectively. Thus, each plane on the cube includes currents of two orthogonal directions. A division scheme of current in direction is shown in Fig. 3.

$$m_{sx} = 2m_x + 2m_y, \quad m_{sy} = 2m_y + 2m_z, \quad m_{sz} = 2m_z + 2m_x$$

2.2. Electric Field Integral Equation (EFIE)

The tangential electrical field on the perfect conductors is zero. The incident field expressions are [1]

$$-\vec{E}^{inc}(\vec{r}) \cdot \hat{s} = \left[-j\omega\vec{A}(\vec{r}) - \nabla\Phi(\vec{r})\right] \cdot \hat{s} \tag{1a}$$

$$-\vec{E}^{inc}(\vec{r}) \cdot \hat{l} = \left[-j\omega\vec{A}(\vec{r}) - \nabla\Phi(\vec{r})\right] \cdot \hat{l} \tag{1b}$$

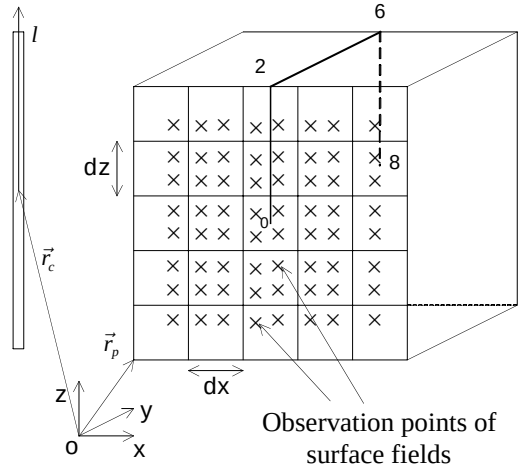

Figure 1. Wire antenna in the presence of a perfect conducting cube.

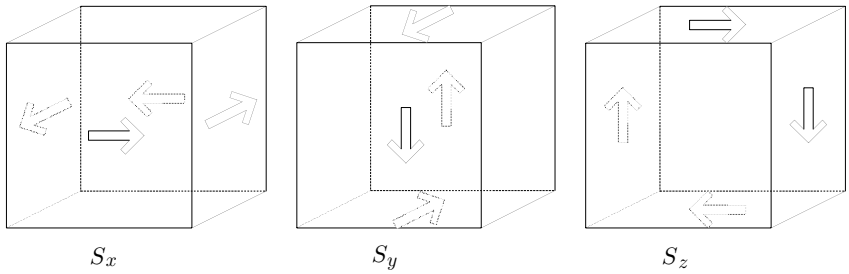

Figure 2. Current flow in the three directions of a conducting cube.

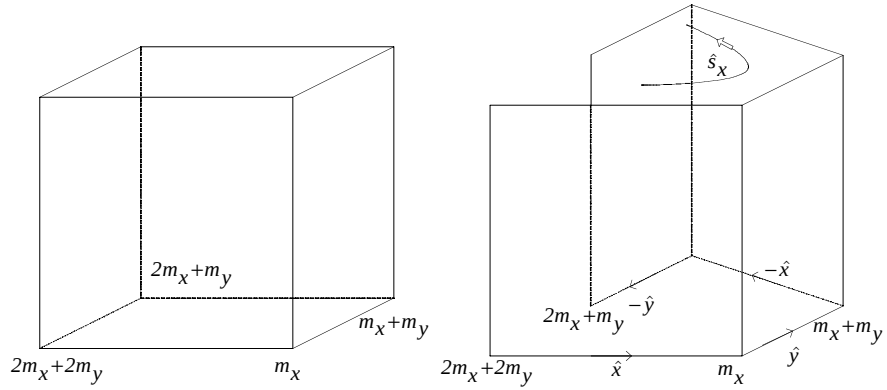

Figure 3. A schematic of the current flow in the direction, $\hat{s}_x$.

where the vector $\vec{r}$ in Eq. (1a) is located on the surface of the conductors; the vector $\vec{r}$ in Eq. (1b) is located on the wire antenna. The potentials are given by

$$\vec{A}(\vec{r}) = \mu \int\limits_{\text{wire}} \vec{I}(l')G_l dl' + \mu \iint\limits_{\text{plane}} \vec{J}(\vec{r}')G_p ds'dy' \tag{2a}$$

$$\Phi(\vec{r}) = \frac{1}{\varepsilon} \int\limits_{\text{wire}} q(l')G_l dl' + \frac{1}{\varepsilon} \iint\limits_{\text{plane}} \rho(\vec{r}')G_p ds'dy' \tag{2b}$$

where $\vec{I}$, $\vec{J}$ are current density on the wire antenna and conductors surface respectively. q and p are electric charge density on the wire antenna and conductors surface respectively and the Green's functions are

$$G_p = \frac{e^{-jk|\vec{r}-\vec{r}'|}}{4\pi|\vec{r}-\vec{r}'|} \tag{3a}$$

$$G_l = \frac{e^{-jk|\vec{r}-\vec{r}_c-l'\hat{l}|}}{4\pi|\vec{r}-\vec{r}_c-l'\hat{l}|} \tag{3b}$$

The current on the wire antenna and the surface patch can be represented as

$$\vec{I}(l) = \sum_{n=1}^{N_l} I_n \Delta\hat{l}_n P_n \tag{4a}$$

$$P_n = \begin{cases} 1, & l_{n-\frac{1}{2}} \sim l_{n+\frac{1}{2}} \\ 0, & \text{others} \end{cases} \tag{4b}$$

where N_l stands for the segment number into which the wire antenna is divided, and the current density is given by

$$\vec{J}(\vec{r}) = \sum_{k=1}^{3} \sum_{n=1}^{m_{a(k)}} \sum_{m=1}^{m_{sk}} J_{sk}^{mn} \hat{s}_k(\vec{r}) P_k^{mn} \tag{5}$$

where $k = 1, 2$ and 3 correspond to x, y and z respectively. For example, when $k = 1$, $m_{a(k)}$, stands for m_x and m_{sk} stands for m_{sx}.

$$a(k) = \begin{cases} 3, & k = 1 \\ 1, & k = 2 \\ 2, & k = 3 \end{cases} \tag{6a}$$

and

$$P_k^{mn} = \begin{cases} 1, & \begin{cases} m - \dfrac{1}{2} \sim m + \dfrac{1}{2} \\ n - 1 \sim n \end{cases} \\ 0, & \text{others} \end{cases} \tag{6b}$$

The electric charge can be represented as

$$q(l) = -\frac{1}{j\omega} \sum_{n=1}^{N_l+1} \frac{I_n - I_{n-1}}{\Delta l_n} P_l^n \tag{7a}$$

$$P_l^n = \begin{cases} 1, & l_{n-1} \sim l_n \\ 0, & \text{others} \end{cases} \tag{7b}$$

$$\rho(\vec{r}) = -\frac{1}{j\omega} \sum_{k=1}^{3} \sum_{n=1}^{m_{a(k)}} \sum_{m=1}^{m_{sk}} \left[\frac{J_{sk}^{mn} - J_{kx}^{m-1,n}}{s_{km} - s_{k(m-1)}} \right] P_{sk}^{mn}(\vec{r}) \tag{8a}$$

$$P_{sk}^{mn} = \begin{cases} 1, & \begin{cases} m - 1 \sim m \\ n - 1 \sim n \end{cases} \\ 0, & \text{others} \end{cases} \tag{8b}$$

Therefore, Eq. (2) become

$$\begin{aligned} \vec{A}(\vec{r}) = {} & \mu \sum_{n=1}^{N_l} I_n \Delta \hat{l}_n \int_{l_{n-0.5}}^{l_{n+0.5}} G_l dl' \\ & + \mu \sum_{k=1}^{3} \sum_{n=1}^{m_{a(k)}} \sum_{m=1}^{m_{sk}} J_{sk}^{mn} \int_{s_{a(k)(n-1)}}^{s_{a(k)(n)}} \int_{s_{k(m-0.5)}}^{s_{k(m+0.5)}} \hat{s}_k(\vec{r}\,') G_p ds' dy' \end{aligned} \tag{9a}$$

$$\begin{aligned} \Phi(\vec{r}) = {} & -\frac{1}{j\omega\varepsilon} \sum_{n=1}^{N_l+1} \frac{I_n - I_{n-1}}{\Delta l_n} \int_{l_{n-1}}^{l_n} G_l dl' \\ & - \frac{1}{j\omega\varepsilon} \sum_{k=1}^{3} \sum_{n=1}^{m_{a(k)}} \sum_{m=1}^{m_{sk}} \left[\frac{J_{sk}^{mn} - J_{sk}^{m-1,n}}{s_{km} - s_{k(m-1)}} \right] \int_{s_{a(k)(n-1)}}^{s_{a(k)(n)}} \int_{s_{k(m-1)}}^{s_{km}} G_p ds' dy' \end{aligned} \tag{9b}$$

2.3. The Matching Procedure

Since point matching is used on thin wire antenna, the so-called 'line' matching is applied to the surface structure. The matching on the $\hat{s}_x$ direction is shown below. The matching function is,

$$\delta_{sx} = \begin{cases} \delta(z - z_{N-0.5}), & s_{x(m-0.5)} \le s_x \le s_{x(m+0.5)} \\ 0, & \text{others} \end{cases} \tag{10}$$

If m, n are the source points and M, N are the observation points, then the expression resulting due to matching procedure is

$$\begin{aligned} -\vec{E}^{inc}\left(M, N-\frac{1}{2}\right)\cdot\Delta\vec{s}_x &= -j\omega\mu\sum_{k=1}^{3}\sum_{n=1}^{m_{a(k)}}\sum_{m=1}^{m_{sk}} J_{sk}^{mn}\int_{s_{a(k)(n-1)}}^{s_{a(k)(n)}}\int_{s_{k(m-0.5)}}^{s_{k(m+0.5)}}\hat{s}_k(\vec{r}\,')\cdot\Delta\vec{s}_x G_p ds'dy' \\ &\quad -j\omega\mu\sum_{n=1}^{N_l} I_n\int_{l_{n-0.5}}^{l_{n+0.5}}\Delta\hat{l}_n\cdot\Delta\vec{s}_x dl' \\ &\quad +\frac{1}{j\omega\varepsilon}\left[\Phi'(s_{x(M+0.5)}, s_{z(N-0.5)}) - \Phi'(s_{x(M-0.5)}, s_{z(N-0.5)})\right] \end{aligned} \tag{11}$$

where

$$\begin{aligned} &\Phi'(s_{x(M+0.5)}, s_{z(N-0.5)}) \\ &\quad = \sum_{k=1}^{3}\sum_{n=1}^{m_{a(k)}}\sum_{m=1}^{m_{sk}}\left[\frac{J_{sk}^{mn} - J_{sk}^{m-1,n}}{s_{km} - s_{k(m-1)}}\right]\int_{s_{a(k)(n-1)}}^{s_{a(k)(n)}}\int_{s_{k(m-1)}}^{s_{km}} G_p ds'dy' \\ &\quad\quad + \sum_{n=1}^{N_l+1}\frac{I_n - I_{n-1}}{\Delta I_n}\int_{l_{n-1}}^{l_n} G_l dl' \end{aligned} \tag{12}$$

$\Phi'(s_{x(M-0.5)}, s_{z(N-0.5)})$ is not shown here because the same principle applies as in Eqs. (11) and (12).

In the procedure shown above, if the source point is located on the edge of the cube, it is necessary to separate the equation to two parts, as shown

$$\begin{aligned} \int_{s_{x(n-1)}}^{s_{xn}}\int_{s_{y(m-0.5)}}^{s_{y(m+0.5)}}\hat{s}(\vec{r}\,')\cdot\Delta\vec{s}G_p ds'dy' = \Bigg\{&\int_{s_{x(n-1)}}^{s_{xn}}\int_{s_{y(m-0.5)}}^{s_{ym}} G_p ds'dy'\hat{s}_-(\vec{r}\,') \\ &\int_{s_{x(n-1)}}^{s_{xn}}\int_{s_{ym}}^{s_{y(m+0.5)}} G_p ds'dy'\hat{s}_+(\vec{r}\,')\Bigg\}\cdot\Delta\vec{s} \end{aligned} \tag{13}$$

2.4. The Treatments of the Singularity

The singularities at the patches along all edges (special singularity) occur in the calculation of $\vec{A}$. However, the singularities on the

plane surfaces (normal singularity) will occur when both $\vec{A}$ and Φ are calculated.

One will encounter the following integral when calculating the normal singularity.

$$\begin{aligned}\int_{-\frac{\Delta s}{2}}^{\frac{\Delta s}{2}}\int_{-\frac{\Delta y}{2}}^{\frac{\Delta y}{2}}\frac{e^{-jk\sqrt{s^2+y^2}}}{\sqrt{s^2+y^2}}dyds &= 4\int_0^{\frac{\Delta s}{2}}\int_0^{\frac{\Delta y}{2}}\frac{e^{-jk\sqrt{s^2+y^2}}}{\sqrt{s^2+y^2}}dyds \\ &= 4\int_0^{\frac{\Delta s}{2}}\int_0^{\frac{\Delta y}{2}}\frac{e^{-jk\sqrt{s^2+y^2}}-1}{\sqrt{s^2+y^2}}dyds \\ &\quad +4\int_0^{\frac{\Delta s}{2}}\int_0^{\frac{\Delta y}{2}}\frac{1}{\sqrt{s^2+y^2}}dyds \qquad (14)\end{aligned}$$

The first part of Eq. (14) belongs to the singularity that can be omitted. The integral in the second part is [1]

$$\begin{aligned}4\int_0^{\frac{\Delta s}{2}}\int_0^{\frac{\Delta y}{2}}\frac{1}{\sqrt{s^2+y^2}}dyds &= 2\cdot\Delta s\cdot\ln\left\{\frac{\Delta y}{\Delta s}+\sqrt{1+\left(\frac{\Delta y}{\Delta s}\right)^2}\right\} \\ &\quad +2\cdot\Delta y\cdot\ln\left\{\frac{\Delta s}{\Delta y}+\sqrt{1+\left(\frac{\Delta s}{\Delta y}\right)^2}\right\} \qquad (15)\end{aligned}$$

When the special singularity is dealt with, it is necessary to split the integral into two parts. Assuming that $s_{k,m}$ is to be on the edge of the object. The first part is

$$\int_{s_{a(k),n-1}}^{s_{a(k),n}}\int_{s_{k,m-0.5}}^{s_{k,m}}G_p ds'dy' = 2\int_0^{\frac{\Delta s}{2}}\int_0^{\frac{\Delta y}{2}}\frac{e^{-jk\sqrt{s^2+y^2}}}{4\pi\sqrt{s^2+y^2}}dsdy \qquad (16)$$

The second part is

$$\int_{s_{a(k),n-1}}^{s_{a(k),n}}\int_{s_{k,m}}^{s_{k,m}+0.5}G_p ds'dy' = 2\int_0^{\frac{\Delta s}{2}}\int_0^{\frac{\Delta y}{2}}\frac{e^{-jk\sqrt{s^2+y^2}}}{4\pi\sqrt{s^2+y^2}}dsdy \qquad (17)$$

The treatment remains the same as that in Eq. (14).

3. THE NEAR FIELDS OF WIRE CURRENT UNIT

A brief introduction to the SEDM method and its application to compute the near fields of wire antennas is presented in this section.

3.1. Series Electric Dipoles Modeling (SEDM) of Wire Current Unit

When solving the wire antenna problem by using MoM, antennas are usually divided into several segments. A single segment with current is defined as wire-current unit. The wire-current unit can be considered as follows: it is connected by many electric dipoles end-to-end with the same current value. This is so-called Series Electric Dipoles Modeling (SEDM).

The electromagnetic fields of the electric dipole, as shown in Fig. 1, are as the follows [6],

$$E_r = \frac{I_0 l}{2\pi} e^{-j\vec{k}\cdot\vec{r}} \left(\frac{\eta}{r^2} + \frac{1}{j\omega\varepsilon r^3} \right) \cos\theta \tag{18a}$$

$$E_\theta = \frac{I_0 l}{4\pi} e^{-j\vec{k}\cdot\vec{r}} \left(\frac{j\omega\mu}{r} + \frac{\eta}{r^2} + \frac{1}{j\omega\varepsilon r^3} \right) \sin\theta \tag{18b}$$

$$H_\varphi = \frac{I_0 l}{4\pi} e^{-j\vec{k}\cdot\vec{r}} \left(\frac{jk}{r} + \frac{1}{r^2} \right) \sin\theta \tag{18c}$$

The above fields are valid under the conditions,

$$l \ll r \qquad d \ll l \tag{19}$$

where d is diameter of the electric dipole. When the condition in Eq. (19) cannot be satisfied, it is necessary to model the wire-current unit as several series dipole segments in order to use Eqs. (18a-c).

3.2. Application of SEDM to Wire Antenna

The SEDM can be used to analyze the near-field problem of wire antennas. Typically, a wire that is about one wavelength is usually divided into about 25 segments [6] when using MoM with pulse expansion point matching technique. For example, a 20 m long wire antenna working on a wavelength of 150 m can be divided into four segments. When one wants to find the fields situated 5 m away, the valid condition in Eq. (19) can not be satisfied, as the segment length is also 5 m long. One can always divide the antennas into more segments to make the segment length shorter. However, this is at the cost of more memory requirement and lower computational efficiency.

In this paper, two novel methods are used to overcome the mentioned shortcomings. They are used to calculate the near and far fields of the wire antenna after their current distribution has been obtained by MoM with traditional segment division method [6]. The two methods are the 'Subdivision with Interpolation' (SI) method and

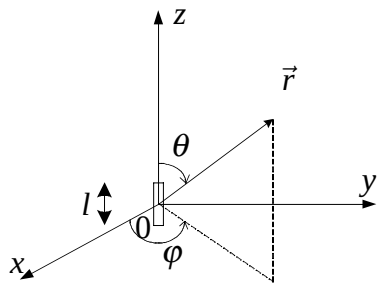

Figure 4. Schematic of a surface current patch.

the 'Subdivision Without Interpolation' (S0I) method. The SI method subdivides the wire current units into segments while ensuring that the satisfaction of the condition in Eq. (19). The current values of the subdivisions are then determined by interpolation. The SOI method is similar to the SI method in terms of its subdivision but does not perform the interpolation process after subdividing the wire current units.

3.3. Comparisons between the SEDM Method and the NEC2 Codes [7]

Table 1 shows the computed results of near fields of a wire antenna using the SEDM method and NEC2 Codes. The radius, operating frequency, and the height of the antenna are 2 mm, 7.5 MHz and 20 m respectively. The coordinate origin is located at the center of the antenna.

Table 1. Near fields results of a wire antenna (V/m).

Items compared	Number of Divisions	Observation Point (1m, 0, 0)			Observation Point (50m, 0, 0)		
		No Subdivision	S0I	SI	No Subdivision	S0I	SI
SEDM	13	548.42	53.49	50.10	6.15	6.11	6.11
	51	51.74	51.47	51.19	6.16	6.16	6.16
NEC2	12	43.00	42.10	—	6.15	6.15	—
	200	51.49	51.45	—	—	—	—

In Table 1, 'No Subdivision' means that Eq. (18) is applied directly after the current distributions obtained by MoM, without further subdividing the wire current units. It is clear that the 'No Subdivision' technique cannot be used when the number of divisions is too small in

both the SEDM method and NEC2 codes. For far field calculations, both the SEDM method and the NEC2 codes are in good agreement even when 'No Subdivision' is used. When one calculates the near-field problem using SOI and SI with the SEDM method, the results agree well with the technique using many more basis functions, even when the divisions as little as 13 segments. For comparison, NEC2 codes produce incorrect results when only 12 segments are used. This shows the validity of the SEDM method, even when the segments are comparable to the field vector length r. For the SEDM method, with 51 segments, the accuracy of the results is sufficient for comparison with the NEC2 code with 200 segments.

4. THE SURFACE AND NEAR FIELDS OF PATCH CELL

A brief introduction to the simplified hybrid method [5] for the calculation of the near and surface fields of objects efficiently is presented here.

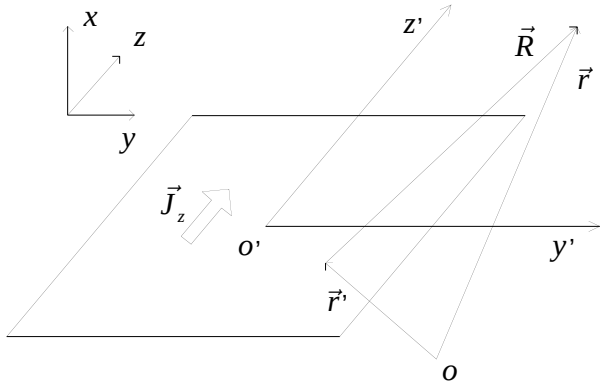

Figure 5. Schematic of a surface current patch for the Kemptner Method.

4.1. SEDM for Surface Current Patches

The electric fields of surface current patches as shown in Fig. 5 can be expressed in Eq. (20) which can be derived from the Stratton-Chu Formula [8].

$$\vec{E}(\vec{r}) = -j\omega\mu \int_s \overline{\overline{G}}(\vec{r}, \vec{r}') \cdot \vec{J}(\vec{r}')ds' \tag{20}$$

With the current on the patch only in the z direction, the Eq. (20) can be simplified to the following double surface integral,

$$E_z = \frac{-j\eta}{k}\left\{\iint_s k^2 J_z G dz'dy' + \iint_s J_z \frac{\partial^2 G}{\partial z^2} dz'dy'\right\} \tag{21}$$

where η is the wave impedance in free space, k is wave number, G is the Green's Function in free space.

In order to avoid the numerical integrals in Eq. (21), the authors have presented a novel method named SEDM for surface current patches. Fig. 6 shows the subdivision of surface patches. The length of the sub-patch (Δl) after the subdivisions should still satisfy the condition in Eq. (19). In fact, good results can be obtained if we let $r \geq 10 \cdot \Delta l$.

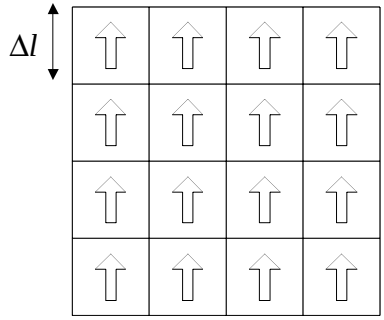

Figure 6. SEDM of surface patch for Kemptner Method.

4.2. Kemptner Method for Surface Field Calculation

The radiated field of the surface current patch shown in Fig. 5 can be expressed as follows [4],

$$\begin{aligned}\vec{E}(\vec{r}) \;=\; & \frac{k^3}{4\pi j\omega\varepsilon}\iint_{s'}\left\{\left[-\frac{1}{k^3R^3}+\frac{1}{2kR}-\frac{j}{2}-\frac{kR}{2}\right]\vec{J}_z + S_1(R)\cdot\vec{J}_z\right. \\ & + \left[\frac{3}{k^3R^3}+\frac{1}{2kR}-\frac{j}{2}+\frac{kR}{2}\right]\frac{(z-z')J_z}{R}\begin{pmatrix} x-x' \\ y-y' \\ z-z' \end{pmatrix} \\ & \left. + S_2(R)\frac{(z-z')J_z}{R}\begin{pmatrix} x-x' \\ y-y' \\ z-z' \end{pmatrix}\right\} dy'dz' \end{aligned} \tag{22}$$

where,

$$S_1(R) = (-1 - jkR + k^2R^2)\frac{e^{-jkR} - \left(1 - jkR - \dfrac{k^2R^2}{2}\right)}{k^3R^3} \quad (23a)$$

$$S_2(R) = (3 + j3kR - k^2R^2)\frac{e^{-jkR} - \left(1 - jkR - \dfrac{k^2R^2}{2}\right)}{k^3R^3} \quad (23b)$$

$$R = \sqrt{(x - x')^2 + (y - y')^2 + (z - z')^2} \quad (23c)$$

One can analytically calculate the integrals terms in Eq. (22), excluding s_1 and s_2. The terms including s_1 and s_2 can be computed by numerical integration since the following limiting value exists,

$$\lim_{R\to 0} \frac{e^{-jkR} - \left(1 - jkR - \dfrac{k^2R^2}{2}\right)}{k^3R^3} = \frac{j}{6} \quad (24)$$

thus ensuring no singular behavior when $R \to 0$.

4.3. Simplified Hybrid Method for Near and Surface Field Calculation

Table 2 shows the computed electric field results and the CPU time required for four observation positions using four different methods. The observation point is located at $(x, 0, 0)$ with reference to the coordinate shown in Fig. 5. A Pentium 450 personal computer is used. The results show that the Kemptner Method takes much longer than the other methods, thus it is very inefficient when applied to all the sub-patches. It can also be seen that the SEDM method is an efficient method for computing near field, however, it cannot be used to obtain the surface fields of patches closest to the observation point.

The novel technique combines the advantages of two methods; the Kemptner Method for the calculation of the sub-patches that are closest to the observation point; the SEDM for the computation of the rest of the sub-patches. The fields can be obtained by vector combination of the above electric and magnetic fields of each sub-patch. The simplified hybrid method has high computational efficiency as can be seen in Table 2.

Table 2. Comparison of the four methods.

E_z &Time (V/m, s)	$x = \lambda$		$x = 0.1\lambda$		$x = 0.01\lambda$		$x = 0\lambda$	
	Value	Time	Value	Time	Value	Time	Value	Time
Double Integral	-1.33-j7.27	<0.01	-27.97+j32.76	0.02	-30.33+j51.92	0.07	—	
SEDM	-1.32-j7.28	<0.01	-27.97+j32.78	0.01	-30.33+j51.92	0.17		
Kemptner Method	-1.33-j7.27	1.21	-27.97+j32.76	0.27	-30.33+j51.92	0.71	-30.36+j42.31	0.38
Simplified Hybrid	-1.33-j7.27	<0.01	-27.97+j32.76	0.01	-30.33+j51.92	0.60	-30.36+j42.31	0.19

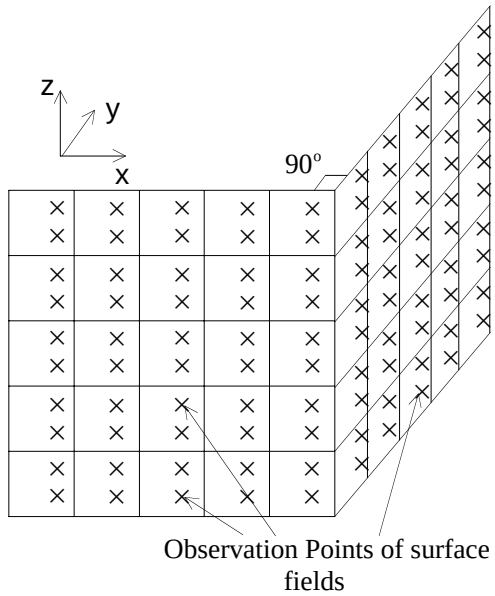

Figure 7. Schematic of a perfect conducting 90 bend structure.

5. NUMERICAL RESULTS

5.1. A Perfect Conducting 90° Bend Structure Irradiated by a Plane Wave

A perfect conducting 90° bend structure as shown in Fig. 7 is irradiated by a plane wave. The size of the structure is λ in all three directions: x, y, z and each direction is divided into 5 segments. The plane wave

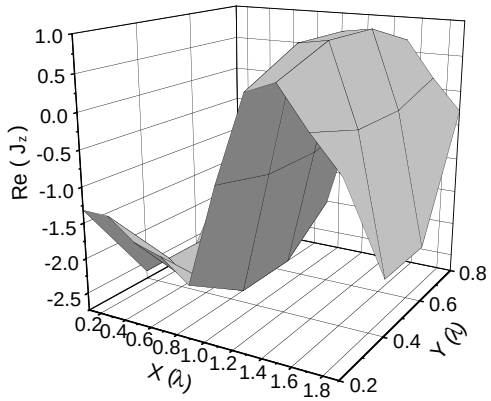

(a)

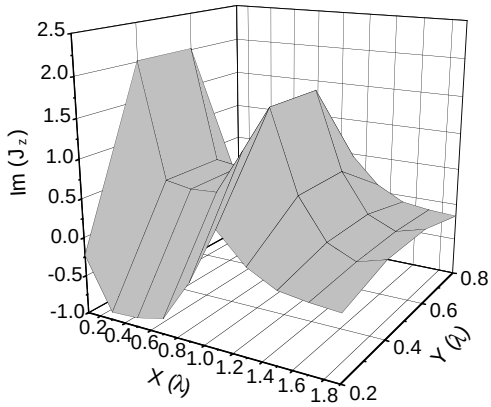

(b)

Figure 8. Current distribution on the bend structure (a) real part of J_z (b) imaginary part of J_z.

is as follows,

$$\vec{E}_z^{inc} = -\hat{e}_z 120\pi e^{-jky} \tag{25}$$

This example is the same as that in Glisson's dissertation [1]. Using Glisson's, the result of the current distribution is as shown in Fig. 8 and is found to be the same as that in the reference. The simplified hybrid calculation method is used to compute the z surface tangential electric field distributions and is plotted in Fig. 9. For this result, the observation points used are located at the positions marked '$\times$' as shown in Fig. 7. Both theoretically and practically, the z tangential

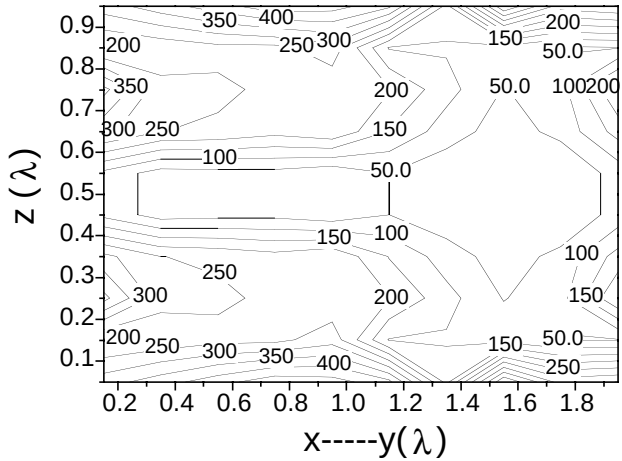

Figure 9. z tangential electric field on the surface of the bend structure.

electric field value on the surface of perfect conducts is zero. However, Fig. 9 shows that when the tangential electric field is calculated using the simplified hybrid method, it is not zero and is rather large especially when the top and bottom of the structure are reached. One of the possible reasons for the discrepancy when using the simplified hybrid calculation is that the pulse expansion used in this method is too rough to model the current distribution on the plane surface of open structures. Nevertheless, this situation is improved when used for closed objects such as cubes. This is shown in the next section.

5.2. A Perfect Conducting Cube Irradiated by a Plane Wave

A perfect conducting cube of size as shown in Fig. 1 is irradiated by a plane wave. The plane wave is as in Eq. (25).

Fig. 10 shows the results of current density along the locus 0268 (Fig. 1) for two cases: 4×4 elements per plane, resulting in 192×192 elements in the impedance matrix; 6×6 elements per plane, resulting in 432×432 elements in the impedance matrix. The results of the two cases are in good agreement with the results obtained by using FDTD method. As expected, the results are better when more segmentations of the object are made.

The x-z plane tangential electric field distributions are calculated by using the simplified hybrid calculation method and results are shown in Fig. 11. The observation points are marked '$\times$' as shown in Fig. 1.

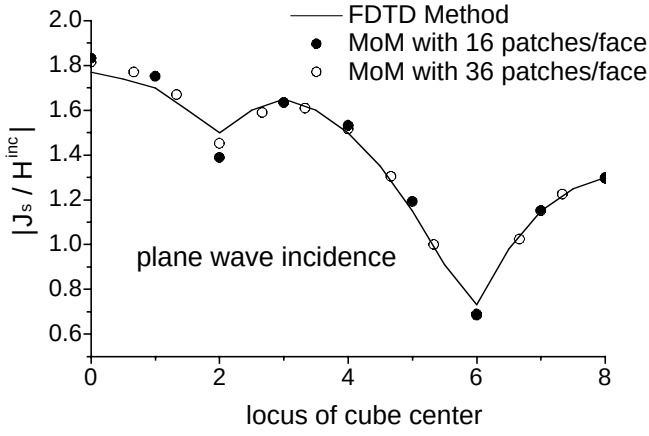

Figure 10. Current densities along 0268.

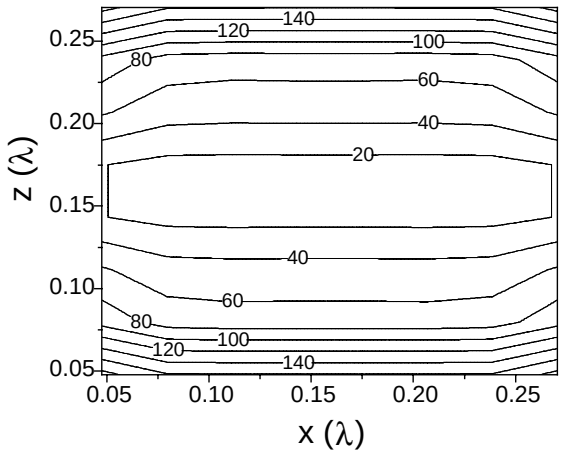

Figure 11. z tangential electric fields on the surface of the cube shown in Fig. 1.

As can be seen, the z tangential electric field is below 100 V/m in most of the patch region and below 50 V/m in the center of the patch region, but becomes larger near the top and bottom edge of the object. Lower values can be achieved by making more segmentation near the edges of the objects. As the plane wave used to irradiate both structures in Fig. 1 and Fig. 7 is the same, the two cases in Section 5.1 and 5.2 can be compared. It is clear that the values in Fig. 11 are much

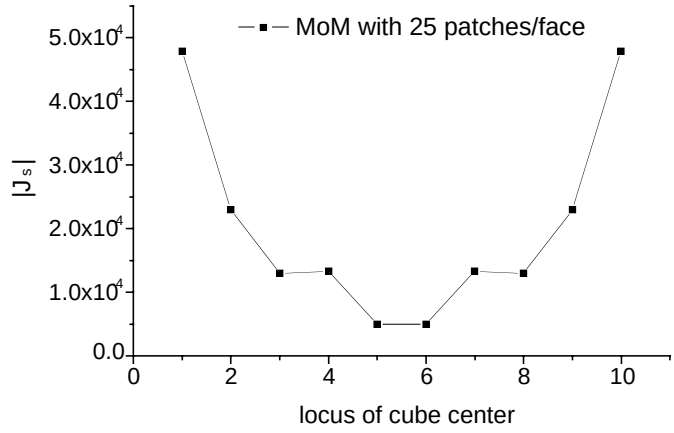

Figure 12. Current densities along 0268.

lower than the values in Fig. 9. Therefore, the pulse expansion point matching technique of MoM is more suitable for the applications to closed objects.

5.3. Center Fed Half-Wave Wire Antenna in the Presence of a Perfect Conducting Cube

Numerical results for a center fed half-wave wire antenna in the presence of a perfect conducting cube as shown in Fig. 1 is shown in Fig. 12 and Fig. 13. The thin wire antenna is 1 m high and the radius of the antenna is 0.0001 m and the location vectors are,

$$\vec{r}_c = (0, 0, 0) \qquad \vec{r}_p = (2m, -0.5m, -0.5) \tag{26}$$

In this case, the total number of elements in the impedance matrix is 325×325, where the wire antenna is divided into 25 sections and 5×5 elements per plane of cube.

At 300 MHz, 1 volt is applied to the input port of the thin wire antenna. The current density along the locus 0268 is shown in Fig. 12. The near field, E_z, on the plane $x = \lambda$ calculated using the simplified hybrid method is shown in Fig. 13. The z tangential electric field on the cube surface is not shown here because its value is only around 0.3 V/m as the input voltage is low. The input impedance of wire antenna is $79.3 + j41.8$ ohms in free space which are very close to the available theoretical value. It becomes $82.2 + j38.4$ ohms for the case of a wire antenna in the presence of a perfect conducting cube. The real part of the input impedance is large due to the presence of the cube.

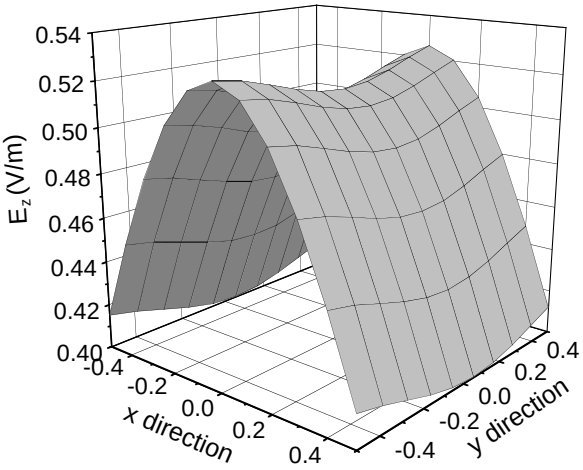

Figure 13. Near electric field on plane $x = \lambda$.

6. CONCLUSION

Near field and surface field analysis of thin wire antennas in the presence of a perfect conducting cube are performed using MoM and EFIE. This paper extended the Glisson's method to the applications of closed objects. Numerical results both for a perfect conducting 90(bend open structure and a perfect conducting closed cube irradiated by a plane wave are in good agreement with the available references. Thus verifying the proposed pulse expansion point matching technique. Furthermore, the tangential electric field distributions for the above two cases obtained by the proposed simplified hybrid calculation method shows that the pulse expansion point matching technique method is more suitable for use with closed object problems as compared to open object problems. The result of a center fed half-wave wire antenna in the presence of a conducting cube is presented. The advantages of using this hybrid method to calculate the near field and surface field of an object is its simplicity and efficiency.

The proposed pulse expansion point matching technique can also be used for solving cases where several wire antennas are in the presence of conducting cubes. Moreover, the proposed method can also be used to solve far field problems. The result is useful for the RF and microwave antenna community.

REFERENCES

1. Glisson, G. W., "On the development of numerical techniques for treating arbitrarily shaped surfaces," Ph.D. Dissertation, University of Mississippi, 1978.
2. Rao, S. M., D. R. Wilton, and G. W. Glisson, "Electromagnetic scattering by surfaces of arbitrary shape," *IEEE Transaction on Antenna Propagation*, Vol. 30, No. 3, 409–418, 1982.
3. Wilkes, D. L. and C. C. Cha, "Method of moments solution with parametric curved triangular patches," *1991 IEEE AP-S Int. Symp. Dig.*, 1512–1515, 1991.
4. Kemptner, E., "Determination of lines of constant phase in the near-field of a metallic cube and an airplane," *IEEE Transaction on Antenna Propagation*, Vol. 42, No. 7, 897–904, 1994.
5. Zhang, X. J., A. Alphones, and A. Q. Liu, "Simplified hybrid calculation method for the surface fields and near fields of surface current patches," *Microwave and Optical Technology Letters*, Vol. 36, No. 6, 471–474, 2003.
6. Bulter, C. M. and D. R. Wilton, "Analysis of various numerical techniques applied to thin-wire scatterers," *IEEE Transaction on Antenna Propagation*, Vol. 23, 534–540, 1975.
7. Burke, G. J. and A. J. Poggio, "Numerical electromagnetic code (NEC) — Method of Moments: Part II: Program description — Code," Lawrence Livermore Laboratory, 1981 (NEC2).
8. Cloud, M. J., *Electromagnetics*, Boca Raton, CRC Press LLC, 2001

X. J. Zhang received his B.Eng., M.Eng., and Ph.D. degrees from Xidian University in 1994, 1997, and 2000, respectively in China. He worked as a Postdoctoral Fellow in the Laboratory of Mobile Communication at the Shanghai Jiaotong University from 2000 to 2002. Currently, he is a Research Fellow at School of Electrical and Electronic Engineering, Nanyang Technology University, Singapore. His research interests focus on computational electromagnetics, antenna and RF IC design, photonic bandgap, and RF MEMS.

A. Q. Liu received his Ph.D. in Applied Mechanics from National University of Singapore (NUS) in 1994. His M.Sc. degree was in Applied Physics, and B.Eng. degree was in Mechanical Engineering from Xi'an Jiaotong University. Currently, he is an Associate Professor at the Division of Microelectronics, School of Electrical & Electronic

Engineering, Nanyang Technological University (NTU). He is also appointed as an Associate Editor and member of the Editorial Board of the IEEE Sensor Journal. His research interests are MEMS design, simulation and fabrication processes in the field of optical and RF MEMS.

Y. H. Lee received her Ph.D. from University of York and joined NTU in 2002. She is currently an Assistant Professor in the School of EEE and a member of IEEE and IEE. Her current research interest includes optimisation based on heuristic techniques, computational electromagnetics and antenna design for electromagnetic compatibility testing purposes.

A. Alphones is Associate Professor at School of Electrical and Electronic Engineering, Nanyang Technology University, Singapore. He has 19 years of research experience. He is a Senior Member of IEEE. He is in the Editorial Board of IEEE Microwave Theory and Techniques and Microwave and Wireless Components Letters. He has published and presented over 70 technical papers in International Journals/Conferences. His current interests are electromagnetic analysis on planar RF circuits and integrated optics, optical-microwave interaction, and hybrid fiber-radio systems.

Changhong Liang graduated from the Department of Radio Physics Northwest Telecommunication Engineering Institute, P. R. China, in 1965. Since 1967 he has been working in the Department of Electromagnetic Engineering at the same university, where he is now a Professor and the president of Xidian University. From 1980 to 1982 he was a Visiting Professor at Syracuse University, Syracuse, NY. He has authored over 100 papers in scientific journals and conferences. His interests include computational electromagnetics, computational microwave, network theory, electromagnetic scattering and electromagnetic soliton. Prof. Liang is a fellow of China Institute of Electronics (CIE), the deputy Chairman of Microwave Society, and the Senior Member of IEEE.